Magnetic Phase Diagram of Alternating Chain Compound $Pb_2V_3O_9$

Kazuhiro NAWA[1]*, Chishiro MICHIOKA[1], Kazuyoshi YOSHIMURA[1] †,
Akira MATSUO[2], and Koichi KINDO[2]

[1]*Department of Chemistry, Graduate School of Science, Kyoto University, Kyoto 606-8502, Japan*
[2]*Institute of Solid State Physics, University of Tokyo, Kashiwanoha, Kashiwa, Chiba 277-8581, Japan*

$Pb_2V_3O_9$ is a quasi one-dimensional compound with antiferromagnetic alternating chains. We measured the magnetization and the specific heat in a single crystal of $Pb_2V_3O_9$ with applied magnetic fields up to 14 T and established the magnetic phase diagram. The phase boundary in the high magnetic field region is in a good agreement with that predicted by the mean field theory in the classical magnetic ordering of the transverse magnetization, while that in the low magnetic field region should be discussed in the viewpoint of the Bose-Einstein condensation of the field induced magnons. Thus, the experimentally determined phase diagram shows the asymmetry, which should be originated in the mixing contribution of excited states as well as in the interchain interactions.

KEYWORDS: $Pb_2V_3O_9$, Bose-Einstein condensation, magnons, alternating chain, field induced magnetic ordering, magnetic phase diagram

1. Introduction

Low dimensionality in quantum spin systems has been a matter of particular interest over some decades since it could lead to novel exotic phenomena. Since the ground state in the low-dimensional system has instabilities with quantum fluctuations, it can be controlled by external fields or impurity effects. A weakly coupled spin gap system is a candidate for exhibiting novel quantum phenomena due to its low dimensionality. In the case of dimer systems without any interdimer interactions, a dimer has the ground state of $|S, S_z\rangle = |0, 0\rangle$ with excited triplet states of $|S, S_z\rangle = |1, 1\rangle, |1, 0\rangle, |1, -1\rangle$. The field dependence of the energy levels is shown in Fig. 1 as solid lines. The external magnetic field splits the degenerated triplet states and reduces the energy gap between the $|0, 0\rangle$ and $|1, 1\rangle$ states. Under the magnetic field, the ground state changes from the $|0, 0\rangle$ to $|1, 1\rangle$ state and spins induced by the field are aligned along the field. In the presence of the additional antiferromagnetic interdimer interactions, the field-induced magnetic moments can exhibit the magnetic ordering of their transverse spin components. The antiferromagnetic long range ordering (AFLRO) in this manner was predicted by the mean field theory.[1)] The AFLRO state was approximated by the ground state of mixed $|0, 0\rangle$ and $|1, 1\rangle$ states. The energy levels of the mixed states derived based on

*E-mail address: knawa@kuchem.kyoto-u.ac.jp
†E-mail address: kyhv@kuchem.kyoto-u.ac.jp

the mean-field magnetic ordering model of the transverse magnetization are shown in Fig. 1 by dashed lines. In addition, the symmetric bell-shape phase boundary can be derived.[1)] The lower critical field H_{c1}, the upper critical field H_{c2} and the maximum transition temperature to AFLRO phase $T_{\max}$ can be calculated from the intradimer and interdimer interactions. At low temperatures, the phase boundary becomes almost perpendicular to H axis. In fact, $TlCuCl_3$,[2,3)] $KCuCl_3$,[4)] $Ba_3Cr_2O_8$,[5)] $Sr_3Cr_2O_8$[6)] and $Pb_2V_3O_9$[7–10)] were found to show the field-induced magnetic orderings. The induced $|1,1\rangle$ excitations would have characteristics of bosons as excited magnons. The AFLRO phase can be interpreted in terms of a Bose-Einstein condensation (BEC) of magnons. The increase of the magnetic susceptivility below the transition temperature is explained by the increase of condensed magnon density. The magnon BEC picture also gives a power-law like critical behavior described as

$$T_c \propto [H_{c1} - H_{c1}(T=0)]^{1/\phi}, \tag{1}$$

where T_c is the transition temperature to AFLRO phase and ϕ is the critical exponent. Most experimental data supported the magnon BEC picture. The critical exponent ϕ was experimentally reported to be between 1.5 and 2.3, while the value was theoretically predicted as 1.5.[2)] Furthermore, from the view of the phase diagram topology, asymmetric $H-T$ phase diagrams was reported in $Sr_3Cr_2O_8$[6)] and $Pb_2V_3O_9$,[8)] while symmetric one was expected because of the particle - hole symmetry even in the case with the BEC model.

$Pb_2V_3O_9$ was first synthesized by the electrochemical reduction of molten PbV_2O_6[11)] and found to have antiferromagnetic alternating chains. The arrangement of the chains in $Pb_2V_3O_9$ is shown in Fig. 2(a) and the alternating chain is illustrated in Fig. 2(b). A magnetic V^{4+} ions with coordinating six oxygen atoms form $V^{4+}O_6$ octahedrons with corner-sharing of oxygen atoms, forming the spin chain with S = 1/2 along the [101] direction. The octahedrons are aligned on a tilt and the distances between adjacent V^{4+} ions change alternatively. Along the $[10\bar{1}]$ direction, $V^{5+}O_4$ tetrahedrons stand between $V^{4+}O_6$ octahedrons. The calculation by the quantitative spin dimer analysis based on tight binding calculations suggested that the V^{4+}-O-O-V^{4+} super-superexchange interactions along the $[10\bar{1}]$ direction were dominant for the antiferromagnetic alternating chain model.[12)] From magnetization measurements, the existence of a spin gap and the phase transition to the AFLRO phase under magnetic fields have been clarified.[7)] Lower and upper critical fields have been determined as $H_{c1} = 4$ T and $H_{c2} = 38$ T, respectively. From the power low behavior of phase boundary, the critical exponent has been determined as $\phi = 1.9$,[7)] or 2.0.[9,10)] In this paper, we report the magnetic phase diagram precisely determined by using a single crystal in order to elucidate the asymmetric $H-T$ phase diagram.

2. Experiments

The polycrystalline sample of $Pb_2V_3O_9$ was prepared by solid state reaction from PbO, V_2O_5 and V_2O_3. The powders were mixed and then sintered at 570 C° for 2 days with intermediate grindings. Single crystals of $Pb_2V_3O_9$ were grown by self-flux and floating zone methods. The crystal growth by self-flux method was made by cooling the sintered sample slowly from 750 C° in an evacuated quartz tube. Glossy crystals were obtained with a maximum size of $0.2 \times 0.5 \times 0.2$ mm^3. By floating zone method, 8 g of powdered sample was molded into a rod under pressure of 400 kgf/cm^2. The rod was sintered at 500 C° for two days in vacuum and then was set to the sample holder under Ar atmosphere of 1 atm. The crystal growth was made by melting the sample rod partially with a crystal growth speed of 0.5 mm/h. The size of obtained glossy crystal is about $2 \times 2 \times 1$ mm^3. A Debye-Scherrer X-ray diffraction measurement was performed to check the purity, and the single crystal X-ray diffraction measurement was done by transmission Laue method to determine the crystal plane, and axes. The magnetic susceptibility was measured by a superconducting quantum interference device magnetrometer. The magnetization curve was measured up to 55 T with a pulse magnet at Ultra High Magnetic Field Laboratory, Institute for Solid State Physics, University of Tokyo. The specific heat was measured by relaxation method under magnetic field up to 14 T.

3. Results

Viewgraphs of single crystals grown by floating zone method are shown in Fig. 3(a). Figure 4 shows the Debye-Scherrer X-ray diffraction patterns. The crashed powders of single crystals were confirmed to be in a single phase. In addition, each single crystal was found to have a single domain by transmission Laue X-ray photographs. The crystal axes of the sample used in measurements of physical properties were determined as shown in Fig. 3(b).

Figure 5(a) shows the temperature dependence of the magnetic susceptibility under the magnetic field of 1 T. The susceptibility does not depend on the field direction so much. This fact suggests that the magnetic anisotropy is not so large that the orbital contribution would be small. To estimate spin interactions, the susceptibility was fitted to the isolated spin dimer model[13] as well as to the antiferromagnetic alternating chain model.[14]The fitting functions are described by

$$\chi_0 = \chi_{\rm spin}(g, J_0, J_1) + \frac{C}{T} + \chi_0, \tag{2}$$

where J_0, J_1, g, C, χ_0 are the intradimer interaction, the interdimer interaction, g-factor, the Curie constant and the temperature independent term, respectively. The values of estimated parameters are shown in Table I. In the case of the isolated dimer, of course, J_1 must be zero. The alternating chain model reproduces the experimental data much better than the isolated dimer model does, indicating the presence of the interdimer interaction. Here, the J_0 and J_1

were determined as 31.5 and 23.0 K, respectively.

The high-field magnetization curve measured at 1.3 K is shown in Fig. 6. The whole behavior is almost consistent with that observed in the previous report using the polycrystalline sample.[8] The critical fields in 1.3 K were determined as $H_{c1} = 4.7$ T and $H_{c2} = 38.4$ T from anomalies in the field derivative of the magnetization curve.

The specific heat was measured to determine the phase diagram precisely. Figure 7 shows the specific heat at temperatures between 0.5 and 6 K with the field applied along or perpendicular to the b^* axis. Below 4.5 K, a λ-type anomaly due to the second order phase transition was observed, which corresponds to the field induced magnetic ordering. With increasing field, the peak shifts to the higher temperature and the intensity is enhanced. The shift of peak by the magnetic field can be explained by the description of BEC of magnons. The critical temperature T_c was determined from the second temperature-derivative of $\{C(H)-C(H=0)\}/T$, where $C(H)$ is the specific heat under the field H. Rough estimation of the entropy changes accompanied by the phase transition was given by integrating $C(H)/T$ after extracting a phonon contribution of $C_{\rm phonon} \sim 2.94\, T^3$ mJ/(K $\cdot$ mol) from $C(H)$, as shown by solid line in Fig. 7. The phonon estimation was made with an assumption that the entropy change in the alternationg chain model agrees with that in the isolated dimer model at high temperatures. The J_0 in Table I was used for the entropy estimation of the isolated dimers. Figure 8 shows the estimated entropy with the field applied along the b^* axis. The entropy estimation with the field perpendicular to b^* axis provides a quite similar result. The entropy is increased with increasing the field and suppressed below T_c. The enhancement by the field results from the reduction of the spin gap and the suppression below T_c indicates the magnetic ordering under the magnetic field. In the field of 6 T, the entropy is estimated as 0.12 J/(K $\cdot$ mol), which corresponds to the 2.1 % of the maximum value $R\ln 2 = 5.76$ J/(K mol) expected for the spin system of S = 1/2. Therefore, the critical magnon density in 6 T ($T_c = 2.1$) can be described as $n_c = 0.021$ and becomes about 10 times larger than that in $TlCuCl_3$[3] at the same temerature. This indicates that more magnons are induced in $Pb_2V_3O_9$ than in $TlCuCl_3$.

The phase diagram was determined as shown in Fig. 9. Whole behavior of the phase boundary does not depend on the field direction. The anisotropic interactions could yield the field-dependence of the phase diagram, and in $Pb_2V_3O_9$, e.g., the Dzyaloshinskii-Moriya interaction could work due to the absence of the inversion symmetry at the center of V^{4+} pairs. In the case of $Pb_2V_3O_9$, however, the weak field-direction dependencies in χ, C and the phase diagram of $Pb_2V_3O_9$ indicate that the anisotropic interactions are small.

4. Discussion

Here we discuss the shape of the phase diagram and its asymmetric behavior in this section. The dashed line in Fig. 9 expresses the phase boundary of the classical transverse magnetic ordered phase, which can be produced by the mean field theory with the interaction parameters

estimated from the $\chi - T$ curve. The spin Hamiltonian of one-dimensional alternating chain is described by

$$\begin{aligned} H &= H_0 + H' \\ H_0 &= J_0 \sum_i \mathbf{s}_{i1} \cdot \mathrm{s}_{i2} - g\mu_B \mathrm{H} \cdot \sum_i (\mathbf{s}_{i1} + \mathbf{s}_{i2}) \\ H' &= J_1 \sum_i \mathbf{s}_{i2} \cdot \mathbf{s}_{i+1\ 1}, \end{aligned} \tag{3}$$

where i represents the notation of the dimer and $i1$ and $i2$ denote the two spins on each dimer. The site i and i+1 locate on the nearest neighbor along the spin chain. The arrangement of the interaction parameters and the notations are shown in Fig. 2(b). The direction of the spin chain is not important in the following discussion. According to the mean field theory, Tachiki and Yamada confined themselves to subspace of the $|1,1\rangle$ and $|0,0\rangle$ states in the vicinity of H_{c1}.[1)] The model Hamiltonian in eq. (3) is rewritten into the following low energy effective Hamiltonian as,

$$\begin{aligned} H &= H_0 + H' \\ &= \frac{N}{2}\left(J_0 + \frac{J_1}{8} - g\mu_B H\right)\mathbf{1} - \frac{1}{2}\left(J_0 + \frac{J_1}{4} - g\mu_B H\right)\sum_i \sigma_{iz} \\ &\quad + \frac{J_1}{16}\sum_i [-2(\sigma_{ix}\sigma_{i+1\ x} + \sigma_{iy}\sigma_{i+1\ y}) + \sigma_{iz}\sigma_{jz}]. \end{aligned} \tag{4}$$

From eq. (4), H_{c1}, H_{c2} and $T_{\max}$ can be estimated as

$$\begin{aligned} H_{c1} &= \frac{1}{g\mu_B}\left(J_0 - \frac{J_1}{2}\right) = 14.2 \text{ T} \\ H_{c2} &= \frac{1}{g\mu_B}(J_0 + J_1) = 38.8 \text{ T} \\ T_{\max} &= \frac{J_1}{4k_B} = 5.8 \text{ K}. \end{aligned} \tag{5}$$

The estimated value of H_{c2} is quite close to the experimental one. The magnetic field at which T_c becomes the highest is estimated to be $H = (H_{c1} + H_{c2})/2 = 26.5$ T, which is also quite close to the experimental value as shown in Fig. 9. In contrast, the estimated H_{c1} deviates largely from the experimental value.

Figure 10 shows the phase boundary focused on the lower critical field H_{c1}. The power law behavior of eq. (1) was predicted in the magnon BEC model. The dashed and solid lines in Fig. 8 are the phase boundaries produced by the fitting to eq. (1). The dashed line is made by fitting the experimental points under 6 K with ϕ confined to the value of 1.5 and the solid line is made by using ϕ as a fitting parameter, which is determined as 2.1. While the critical exponent ϕ is expected to be 1.5 in the magnon BEC model, the experimental data are better explained by $\phi = 2.1$ with $H_{c1} = 3.4$ T. In early papers, the critical exponent exhibits $\phi = 1.9$,[7)] or

2.0[9,10] and the possibility of ϕ convergence to the universal value $\phi = 1.5$ was suggested in the low-temperature limit, which was first observed in the experimental phase boundary of $TlCuCl_3$. The BEC theory by using realistic dispersion relations of $TlCuCl_3$ explained the phase boundary below 5 K and $\phi = 1.5$ was obtained from fitting in the temperature range below 2.4 K.[3] Also in the case of $Pb_2V_3O_9$, the valid description of the magnon dispersion should be necessary for the universality of AFLRO phase.

To evaluate the magnon-magnon interactions more correctly, we took into consideration the additional effects of the $|1,0\rangle$ and $|1,-1\rangle$ states. In the subspace of the $|0,0\rangle$ and $|1,1\rangle$ states, a point inversion symmetry $h_{\rm eff} \to -h_{\rm eff}, \sigma \to -\sigma$ in Hamiltonian eq. (4) ensures the symmetry of the phase diagram for a zeropoint of the effective field $h_{\rm eff} = h - J_0 - J_1/4$. Second-order processes between the $|0,0\rangle$, $|1,1\rangle$ states and the excited $|1,0\rangle$, $|1,-1\rangle$ states yield the perturbation terms and they break the inversion symmetry in the spin Hamiltonian. The mixing effect with the excited states was discussed in Refs. 15 and 16. In these references, a bond-operator technique was used to describe both the spin-liquid and the ordered states in the field and pressure induced quantum phase transition in $TlCuCl_3$. The values of H_{c1} and H_{c2} were described by intradimer and interdimer interactions, and magnetization curves and the magnon dispersion relations observed in $TlCuCl_3$ were accounted for by the bond-operator technique. In this theory, the operators which correspond to creations and annihilations of the $|0,0\rangle$, $|1,1\rangle$, $|1,0\rangle$ and $|1,-1\rangle$ states represent spin degrees of freedom on each dimer. The interdimer interactions yield the mixed ordered states which are approximated by a linear combination of the $|0,0\rangle$, $|1,1\rangle$ and $|1,-1\rangle$ states. The $|1,0\rangle$ state does not contribute its term to the mixed states. In consideration of the mixing contribution of the $|1,-1\rangle$ state with the $|0,0\rangle$ and $|1,1\rangle$ states, H_{c1} of $Pb_2V_3O_9$ is obtained as

$$H_{c1} = \frac{1}{g\mu_B}\left(\sqrt{J_0^2 - J_0 \cdot J_1}\right) = 11.7 \text{ T} \tag{6}$$

and H_{c2} becomes exactly the same as that in eq. (5). The H_{c2} in eq. (5) agrees with the experimental H_{c2}. The H_{c1} in eq. (6) is smaller than that in eq. (5) and becomes closer to the experimental H_{c1}. The asymmetric behaviors especially in the vicinity of H_{c2} and H_{c1} are due to the change in mixing contribution of the $|1,-1\rangle$ state. Around H_{c2}, the mixing contribution is ignorable and therefore the magnon-magnon interactions in the high field region can be described by quasi one-dimensional mean field. In the vicinity of H_{c1}, the finite mixing contribution reduces the minimum of the magnon dispersion and makes H_{c1} smaller than the value in eq. (5). In addition, magnon-magnon interactions are well described by interacting dilute bosons and therefore the phase boundary shows power-law behavior. The alternating chain model with the field-induced magnetic ordering explains the physical properties of $Pb_2V_3O_9$ very well. Details of AFLRO state in $Pb_2V_3O_9$, especially the critical exponent, may be explained with the modified alternating chain model by additional small

interchain interactions. The experimental H_{c1} is reproduced well if the value of J_1 is regarded as 30.5 K. Since the assumed J_1 is not so different from that estimated from $\chi - T$ curve, the presence of interdimer interactions may increase J_1 and also affect the critical exponent.

5. Conclusion

In summary, the magnetic phase diagram of $Pb_2V_3O_9$ was determined precisely from the high field magnetization and the specific heat by using single crystal. The experimental phase boundary near H_{c2} coincides with that based on the mean field picture, while that in the vicinity of H_{c1} shows the power-law behavior predicted in the magnon BEC picture. These results indicate that the mixing contribution of excited states with low-lying states shifts the phase boundary to the lower field especially in the case of H_{c1}.

Acknowledgments

We thank Dr. T. Waki for helpful discussion and provision of V_2O_3 samples. The single crystal X-ray diffraction measurement was carried out using facilities of Research Center for Low Temperature and Materials Sciences, Kyoto University. This work was supported by a Grant-in-Aid for Scientific Research from the Japan Society for Promotion of Science (19350030, 22350029) and by Global COE Program of Kyoto University, "International Center for Integrated Research and Advanced Education in Materials Science", from the Ministry of Education, Culture, Sports, Science and Technology of Japan.

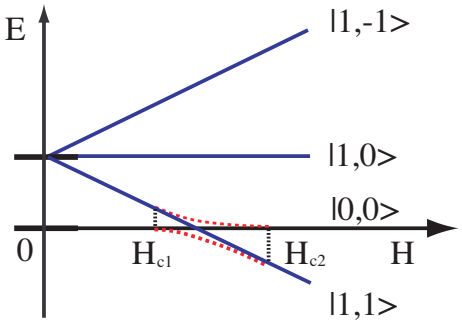

Fig. 1. (Color online) Energy levels of the spin states of $|S, S_z\rangle = |0, 0\rangle$, $|1, 1\rangle$, $|1, 0\rangle$ and $|1, -1\rangle$ in the dimers without any interdimer interactions (solid lines) and the mixed $|S, S_z\rangle = |0, 0\rangle$ and $|1, 1\rangle$ states in interacting dimers derived by the mean field theory (dashed lines).[1)]

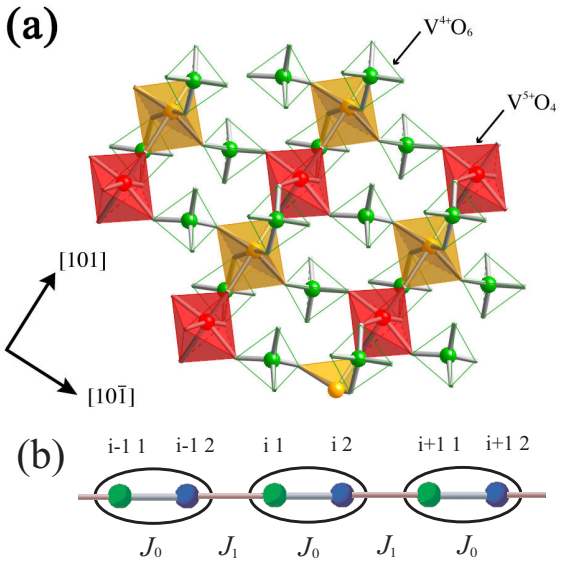

Fig. 2. (Color online) (a) The arrangement of $V^{4+}O_6$ octahedrons and $V^{5+}O_4$ tetrahedrons in the ac plane. (b) The illustration of the alternating chain with the notations above and the interaction parameters below the chain, both of which are used in eq. (3)(see text).

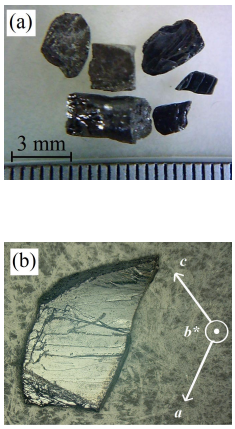

Fig. 3. (Color online) (a) Viewgraphs of single crystals obtained by floating zone method. (b) Crystal axes of the single crystal determined by transmission Laue method.

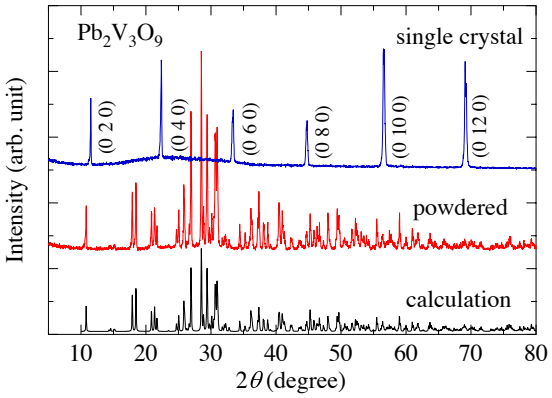

Fig. 4. (Color online) Debye-Scherrer X-ray diffraction patterns for the single and powdered crystals with calculated powder pattern for comparison.

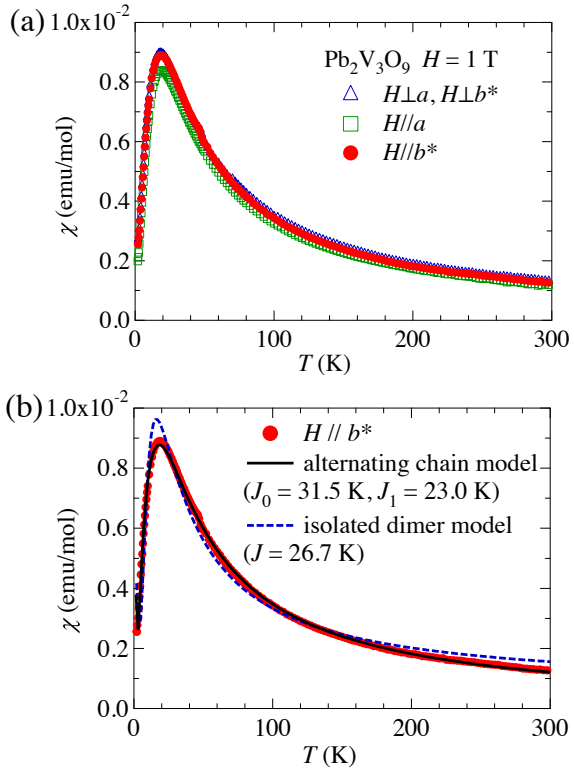

Fig. 5. (Color online) (a) Temperature dependence of magnetic susceptibility under the applied field of 1 T parallel and perpendicular to a, b^* axes. (b) Temperature dependence of magnetic susceptibility with $H \parallel b^*$ (closed circles). Dashed and solid lines show the fitted lines with the isolated dimer[13] and the alternating chain[14] models, respectively.

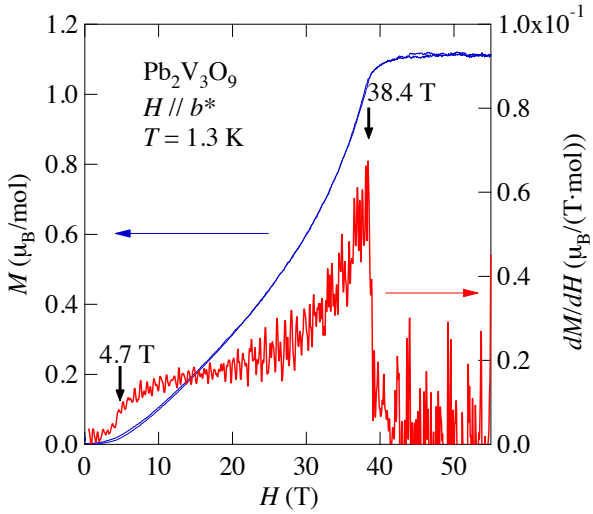

Fig. 6. (Color online) Field dependence of the magnetization with the field $H \parallel b^*$. Critical field is determined as an anomaly field of first derivative in magnetization curves.

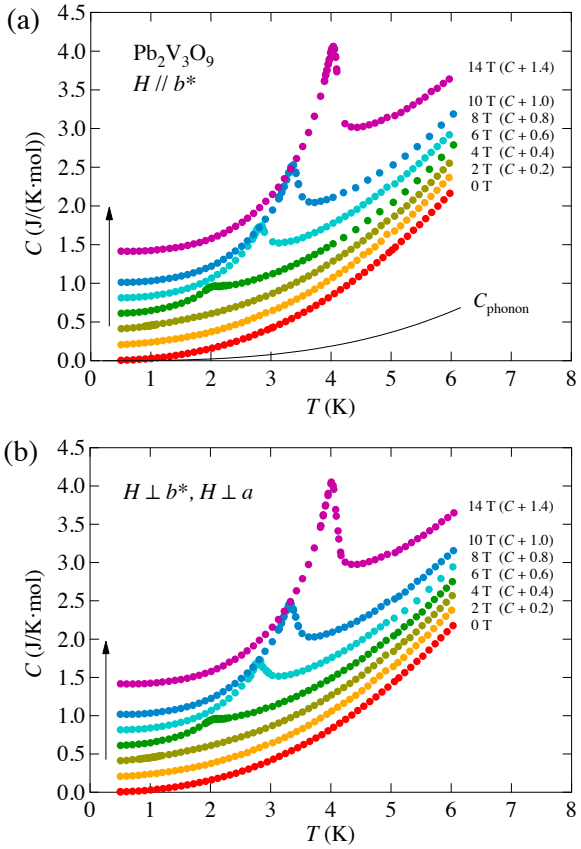

Fig. 7. (Color online) Temperature dependences of specific heats with the field (a) $H \parallel b^*$ and (b) $H \perp b^*$, with offset of $H \times 0.1$ J/(K · mol). Solid line shows the phonon contribution.

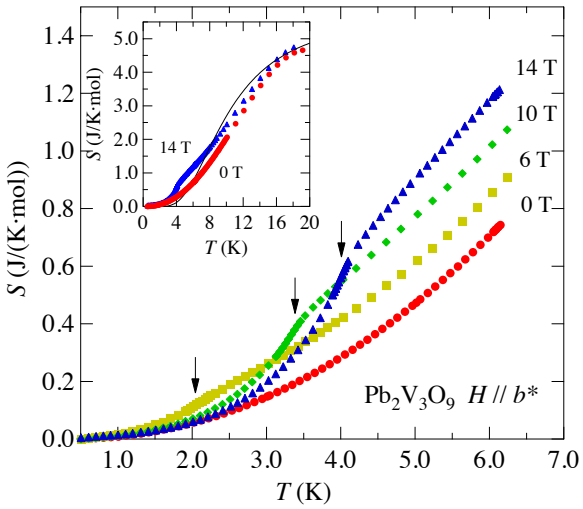

Fig. 8. (Color online) Temperature dependence of magnetic entropy with the field $H \parallel b^*$. Solid arrow indicates T_c at each field. Solid line in inset shows the magnetic entropy of the isolated dimer with the spin gap $\Delta = 26.7$ K under zero field.

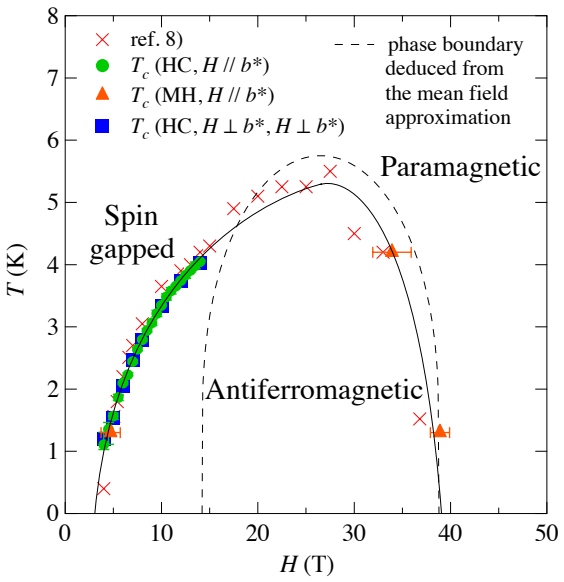

Fig. 9. (Color online) The $H-T$ magnetic phase diagram of $Pb_2V_3O_9$. Solid line is a guide for eyes. Dashed line corresponds to deduced phase boundaries from classical mean field approximation[1)] based on the parameters in Table I.

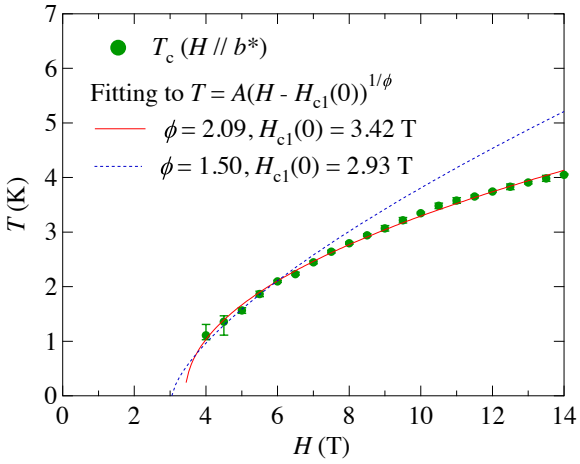

Fig. 10. (Color online) Magnetic phase diagram focused on at low temperatures and in the low field region. Dashed and solid lines are obtained by power law as $T = A(H - H_{c1}(T = 0))^{1/\phi}$ with critical exponent $\phi = 1.50$ and $\phi = 2.09$, respectively.

Table I. Parameters obtained from fitting the magnetic susceptibility to the isolated dimer[13] and the alternating chain[14] models.

	Isolated dimer	Alternating chain
J_0 (K)	26.7 ± 0.3	31.5 ± 0.1
J_1 (K)	-	23.0 ± 0.9
g	1.75 ± 0.02	2.09 ± 0.01
C (emu $\cdot$ K/mol)	$(6.78 \pm 0.47) \times 10^{-3}$	$(5.86 \pm 0.13) \times 10^{-3}$
χ_0 (emu/mol)	$(6.04 \pm 0.61) \times 10^{-4}$	$(-1.08 \pm 0.18) \times 10^{-4}$

References

1) M. Tachiki and T. Yamada: J. Phys. Soc. Jpn. **28** (1970) 1413
2) T. Nikuni, M. Oshikawa, A. Oosawa, and H. Tanaka: Phys. Rev. Lett. **84** (2000) 5868
3) F. Yamada, T. Ono, H. Tanaka, G. Misguich, M. Oshikawa, and T. Sakakibara: J. Phys. Soc. Jpn. **77** (2008) 013701
4) A. Oosawa, T. Takamasu, K. Tatani, H. Abe, N. Tsujii, O. Suzuki, H. Tanaka, G. Kido, and K. Kindo: Phys. Rev. B **66** (2002) 104405
5) M. Kofu, H. Ueda, H. Nojiri, Y. Oshima, T. Zenmoto, K. C. Rule, S. Gerischer, B. Lake, C. D. Batista, Y. Ueda, and S.-H. Lee: Phys. Rev. Lett. **102** (2009) 177204
6) A. A. Aczel, Y. Kohama, C. Marcenat, F. Weickert, M. Jaime, O. E. Ayala-Valenzuela, R. D. McDonald, S. D. Selesnic, H. A. Dabkowska, and G. M. Luke: Phys. Rev. Lett **103** (2009) 207203
7) T. Waki, Y. Morimoto, C. Michioka, M. Kato, H. Kageyama, K. Yoshimura, S. Nakatsuji, O. Sakai, Y. Maeno, H. Mitamura, and T. Goto: J. Phys. Soc. Jpn. **73** (2004) 3435
8) T. Waki, N. Tsujii, Y. Itoh, C. Michioka, K. Yoshimura, O. Suzuki, H. Kitazawa, and G. Kido: Physica B **398** (2007) 148
9) T. Kawamata, N. Sugawara, M. Uesaka, N. Kaneko, T. Kajiwara, H. Yamane, K. Koyama, K. Kudo, N. Kobayashi, and Y. Koike: J. Phys.: Conf. Ser. **150** (2009) 042087
10) B. S. Conner, H. D. Zhou, Y. J. Jo, L. Balicas, C. R. Wiebe, J. P. Carlo, Y. J. Uemura, A. A. Aczel, T. J. Williams, and G. M. Luke: Phys. Rev. B **81** (2010) 132401
11) O. Mentre, A.-C. Dhaussy, F. Abraham, and H. Steinfink: J. Solid. State. Chem. **140** (1998) 417
12) O. Mentre, H.-J. Koo, and M.-H. Whangbo: Chem. Mater. **20** (2008) 6929
13) B. N. Figgis and R. L. Martin: J. Chem. Soc., **1956**, 3837
14) D. C. Johnston, R. K. Kremer, M. Troyer, X. Wang, A. Klümper, S. L. Bud'ko, A. F. Panchula, and P. C. Canfield: Phys. Rev. B **61** (2000) 9558
15) M. Matsumoto, B. Normand, T. M. Rice, and M. Sigrist: Phys. Rev. Lett. **89** (2002) 077203
16) M. Matsumoto, B. Normand, T. M. Rice, and M. Sigrist: Phys. Rev. B **69** (2004) 054423